Observations of Rossby Waves Linked to Convection over the Eastern Tropical Pacific

GEORGE N. KILADIS

Aeronomy Laboratory, NOAA/ERL, Boulder, Colorado

(Manuscript received 18 October 1996, in final form 1 May 1997)

ABSTRACT

Rossby wave activity propagating into the eastern tropical Pacific from the midlatitudes during northern winter is examined in some detail. These waves are associated with the intrusion of high potential vorticity air into low latitudes, and they modulate cloudiness, stability, and vertical motion in the vicinity of the ITCZ. In the upper troposphere and lower stratosphere the horizontal phase and group propagation of the wave activity are qualitatively like those of a nondivergent barotropic Rossby wave. As the waves move equatorward, they become more shallow and propagate upward into the stratosphere. The horizontal and vertical propagation is consistent with the tilts of the waves, the large-scale three-dimensional background flow, and with the signatures of momentum and heat fluxes associated with the wave activity.

In the lower troposphere, paired cyclonic anomalies on either side of the equator accompany the upper level wave activity to the west of the ITCZ cloudiness signal. These waves amplify following the peak in the ITCZ cloudiness and propagate westward along the equator. This suggests that the upper-level wave activity, and possibly the associated convective heating, can trigger the excitation of the equatorially trapped Rossby modes.

The transient wave activity appears to be a crucial component of the momentum balance of the eastern tropical Pacific circulation. There is substantial interannual variability in the wave activity, consistent with observed changes in the large-scale basic state associated with the Southern Oscillation.

1. Introduction

The propagation of Rossby wave energy into the Tropics from higher latitudes is a well-documented feature of the general circulation of the atmosphere. It was realized long ago that such stationary and transient eddies are necessary features of the momentum balance of the atmosphere, since the Hadley circulation alone is incapable of accomplishing the necessary poleward transport of westerly momentum at low latitudes (Jeffreys 1926). Starr (1948) recognized that this transport could be achieved primarily by positively tilted eddies in the subtropics and extratropics, which because of their orientation are also associated with an equatorward propagation of wave energy. Both the stationary and transient eddy fluxes of momentum are important in budgets of atmospheric angular momentum over a broad range of timescales (e.g., Newell et al. 1972; Weickmann et al. 1997).

In addition to the requirements of the momentum balance, disturbances originating in the extratropics are also thought to be an important source for driving tropical motions (e.g., Mak 1969; Zangvil and Yanai 1980; Yanai and Lu 1983; Wilson and Mak 1984; Zhang and Webster 1992; Magaña and Yanai 1995). In particular, Rossby wave activity propagating into the Tropics is observed to occur in local regions of westerly flow that extend from the extratropics into low latitudes (e.g., Kiladis and Weickmann 1992a,b, 1997; Hsu and Lin 1992; Tomas and Webster 1994). This wave energy often disperses across the equator into the Southern Hemisphere, in agreement with theoretical arguments concerning propagation through regions of upper-level equatorial westerlies referred to as ''westerly ducts'' (Webster and Holton 1982). Such regions are particularly well-developed over the equatorial eastern Pacific and Atlantic sectors during northern winter and spring (Kiladis and Weickmann 1997). Arkin and Webster (1985) found a strong relationship between the perturbation kinetic energy (PKE) of the zonal wind and the occurrence of equatorial westerlies at upper levels, such that the PKE was higher in westerlies than in easterlies of the same magnitude on seasonal and interannual timescales. This provides compelling observational support for the idea that low-latitude westerlies are more favorable environments for the forcing of tropical motions by extratropical disturbances than are easterlies.

In a study of relationships between tropical convection and large-scale circulation at 200 mb, Kiladis and Weickmann (1992a,b) demonstrated that high-level cloudiness in the eastern tropical Pacific ITCZ during northern winter was modulated by upper-level Rossby wave activity. This relationship is such that low values

Corresponding author address: Dr. George N. Kiladis, Aeronomy Laboratory, NOAA, R/E/AL3, 325 Broadway, Boulder, CO 80303-3328.
E-mail: gkiladis@al.noaa.gov

of outgoing longwave radiation (OLR) tend to occur ahead of upper-level troughs propagating into the Tropics from the vicinity of the Asian jet exit region. These OLR signals typically evolve into ''cloud band'' signatures in the southwesterly flow ahead of the troughs, of the type seen on satellite photos extending from the ITCZ into western North America (e.g., McGuirk et al. 1987; McGuirk et al. 1988; Iskenderian 1995). In a case study by Kiladis and Weickmann (1992b), the ITCZ convection was associated with the advection of high potential vorticity (PV) air into the Tropics, with upward motion observed in the region of positive PV advection. Tomas and Webster (1994) also identified strong PV signals in conjunction with cross-equatorial wave activity during northern winter.

The signature of equatorward-propagating Rossby wave activity associated with ITCZ convection is also evident in the eastern Pacific during northern spring, and in the Atlantic during northern winter, when belts of upper tropospheric westerlies extend from high latitudes to equatorial regions. During northern summer and fall, when deep equatorial easterlies are present in these regions, the wave activity is absent during periods of low OLR (Kiladis and Weickmann 1997), consistent with the presence of a ''critical line'' to Rossby wave propagation. Since this occurs where the zonal phase speed of a Rossby wave is equal to the background zonal wind, a critical line for a nonstationary Rossby wave of a certain scale may not be present for waves of other scales having different intrinsic phase speeds (Yang and Hoskins 1996).

Of course, ITCZ convection is known to be influenced by many disturbances other than those associated with upper-level Rossby waves. An entire family of equatorially trapped modes predicted theoretically by Matsuno (1966) is observed to be associated with tropical convection (Takayabu 1994). These include mixed Rossby–gravity waves (e.g., Zangvil and Yanai 1981; Liebmann and Hendon 1990) and equatorial Rossby waves (e.g., Kiladis and Wheeler 1995), both of which are westward propagating and modulate off-equatorial convection. Important questions concerning the sources of the energy responsible for the generation of these disturbances have yet to be fully resolved. Webster and Chang (1988) and Chang and Webster (1990, 1995) argue on theoretical grounds that the basic state over the eastern tropical Pacific during northern winter should favor the ''accumulation'' of equatorial wave energy in the zonal direction as well as provide a favorable environment for meridional propagation of extratropical wave activity. However, it appears that the importance of the longitudinal tropical source is negligible compared to the extratropical source, at least for Rossby modes.

In this paper the behavior of upper-level Rossby wave activity of the type documented by Kiladis and Weickmann (1992a,b, 1997) and Tomas and Webster (1994) is examined in some detail. We follow an observational approach similar to those studies by exploiting a regression technique between circulation indices and OLR. Our intent is to document the typical horizontal and vertical structure associated with Rossby waves propagating into the Tropics over the eastern Pacific during northern winter (hereafter referred to as ''wave activity''). Section 2 details the data and methodology used, and the horizontal structure and propagation of the wave activity are described in section 3. The vertical structure and propagation are examined in section 4, and some statistics describing the two-way interaction between the waves and the slowly varying large-scale flow are presented in section 5. Some implications of our findings with respect to the spectrum of precipitation in the ITCZ and also the generation of equatorial Rossby waves are summarized in section 6.

2. Data and methodology

For this study, National Centers for Environmental Prediction (NCEP, formerly the National Meteorological Center) reanalysis data are used to represent the large-scale circulation, and OLR is utilized as a proxy for deep convection. Both of these datasets are on a 2.5° latitude–longitude grid. The original twice-daily OLR data have been interpolated in space and time to yield a global set with no missing data during the study period (Liebmann and Smith 1996). The reanalysis data provide a consistently derived set that is not subject to operational constraints nor changes in the assimilation system (Kalnay et al. 1996). Four times daily grids were averaged to produce a daily reanalysis set for this study, utilizing winds and temperature on 14 pressure levels from 1000 to 50 mb. The 15-season study period spans from December to February (DJF) 1979/80 to 1994/95.

A linear regression technique, described in detail by Kiladis and Weickmann (1992a), is used to examine the horizontal and vertical structure of the typical modes of circulation associated with deep convection over the eastern Pacific during the DJF season. Perturbation quantities are calculated by removing the first three harmonics of the daily means of the entire dataset. Temporal filtering of the data is accomplished by using a Lanczos digital filter with 121 daily weights, giving very sharp response cutoffs with negligible Gibbs oscillation.

Kiladis and Weickmann (1992b) showed that the equatorward-propagating Rossby wave activity was present in both the 6–14-day and 14–30-day band, so we have combined these and here concentrate on variability with periods in the 6–30-day range. The same band was also used by Tomas and Webster (1994). This filtering excludes fluctuations due to the tropical 30–60 day or Madden–Julian oscillation (MJO; see Madden and Julian 1994) and mixed Rossby–gravity waves along the equator (Liebmann and Hendon 1990; Magaña and Yanai 1995), as well as much of the extratropical baroclinic wave activity with periods of less than 6 days. This band is still very broad and contains roughly half

the intraseasonal variance in both OLR and circulation over the study region once the seasonal and diurnal cycles are removed (see Fig. 2 in Kiladis et al. 1994). By contrast, the greater than 30-day timescale only accounts for roughly 20% of the total variance in these parameters.

Power spectra of OLR and 200-mb vorticity over the tropical eastern Pacific ITCZ were calculated using DJF data for the study period (not shown), and it was found that there was an enhancement of power in the 10–15-day range, with the coherence between OLR and vorticity highly statistically significant at these periods. This also is in agreement with spectral and correlation results of Tomas and Webster (1994), who show an average 12-day periodicity in Rossby wave activity propagating across the equator in the same region.

To establish the relationship between deep convection and circulation, filtered OLR data in a selected 10° box base region are regressed against identically filtered u and ν components of the wind and temperature at each global grid point. This procedure yields a separate regression equation between OLR in the base region and the wind and temperature for each global grid point at each pressure level. The linear dependence of the circulation and temperature can then be mapped by applying the regression equation for each grid point using an arbitrary deviation in OLR at the base region as the independent variable. The correlation coefficient enables the statistical significance of the local linear relationship between OLR in the base region and the dependent variable at any given grid point to be assessed. The OLR predictor is also regressed against OLR at all other grid points. Lagged regression relationships can be used to examine the evolution of the convective and circulation signals over time.

From the regressed winds and temperatures at multiple levels, derived quantities such as divergence and PV can also be calculated for a given OLR perturbation in the base region. Gradients are calculated using centered finite differencing, and the velocity potential and streamfunction are obtained by calculating the inverse Laplacian of the global divergence and vorticity fields, respectively.

Negative anomalies in OLR generally occur during periods of high-level cloudiness, and the reconstructed circulations are meant to represent those associated with deep convection at the base region. In the case study examined by Kiladis and Weickmann (1992b), a large region of OLR less than 220 W m^{-2} was observed within the ITCZ. This corresponds to an OLR anomaly of less than -40 W m^{-2} with respect to the DJF long-term mean at that location. For the purposes of the present study, we scale the regressions to a value of -40 W m^{-2} to produce realistic amplitudes of the circulations associated with precipitation events within the ITCZ.

McGuirk et al. (1988) found that the European Centre for Medium-Range Weather Forecasts (ECMWF) and NCEP analyses differed greatly in their depiction of the synoptic-scale structure of the same individual disturbance giving rise to a cloud band over the eastern tropical Pacific. Since these datasets suffer from a lack of rawinsonde observations over the tropical oceans, operational analyses must be used very cautiously for case study purposes of events in these regions. However, as we have shown in several previous studies, the statistical approach outlined here produces robust results that take advantage of the wealth of satellite-derived and aircraft observations assimilated into the reanalysis dataset. In addition, we are able to produce nearly identical results using analyses from ECMWF, so we are quite confident of the qualitative aspects of our conclusions. Further discussion of the statistical significance of the results can be found in Kiladis and Weickmann (1992a, 1997).

3. Horizontal structure

a. 200 mb

In this section we examine the horizontal structure of the synoptic-scale circulation at 200 and 850 mb associated with ITCZ convection during northern winter. Although these circulations are isolated using OLR as a predictor, it will be shown that these modes are quite typical of the type of equatorward-propagating wave activity discussed, for example, by Hsu and Lin (1992) and Tomas and Webster (1994) using circulation parameters as a predictor. The presentation here is based on regression relationships obtained using 6–30-day filtered OLR averaged over the region 5°–15°N, 150°–140°W. As will be shown below, this is near the longitude of maximum upper-level wave activity in the eastern tropical Pacific during DJF, and the results are representative of the entire sector between about 170° to 120°W.

Figure 1 shows the sequence of 200-mb streamfunction and wind anomalies scaled to a -40 W m^{-2} OLR deviation averaged over the base region, which is located within the shaded region on day 0 in Fig. 1c. In these plots, wind vectors are shown only at those points where the correlation coefficients imply statistical significance at better than the 5% level. The theoretical group propagation of a stationary Rossby wave on a sphere in an atmosphere with constant angular velocity is along a great circle (e.g., Karoly and Hoskins 1982). For later reference, a portion of a great circle route is shown in Fig. 1, having a northern turning point at 30°N, 160°E and crossing the equator at 110°W. Also shown is a meridionally oriented line along 145°W, for use in vertical cross sections below.

Four days prior to the peak in ITCZ convection (day -4, Fig. 1a), statistically significant circulations are confined to the western North Pacific and eastern Asia, with an anticyclonic anomaly over southern China tied to enhanced westerlies near the mean position of the Asian jet entrance region. Near the date line there is a trough south of and a ridge north of the Asian jet axis,

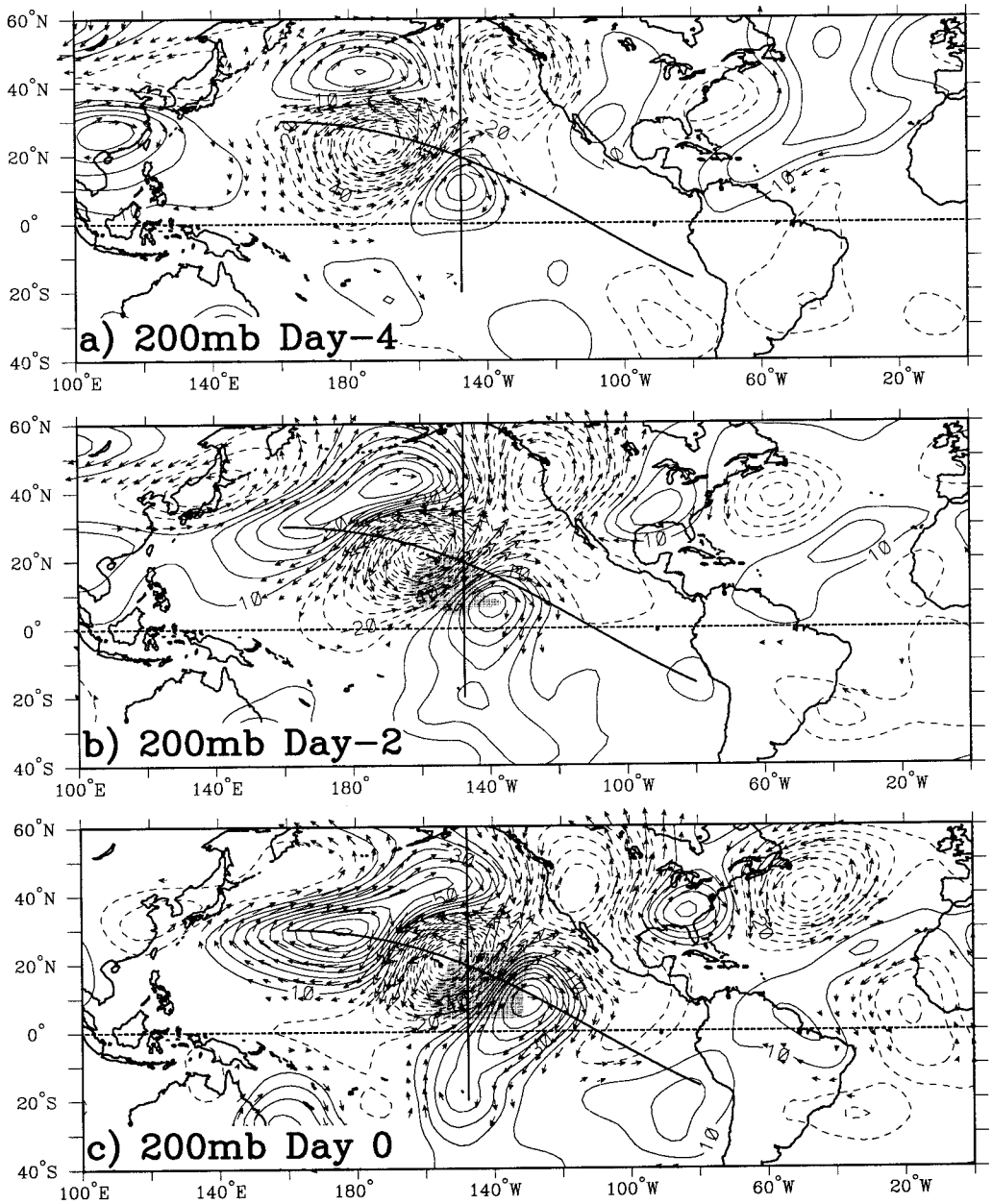

FIG. 1. 6–30-day 200-mb streamfunction, wind, and OLR perturbations associated with a -40 W m^{-2} deviation in OLR in the region 5°N–15°N, 150°–140°W during DJF 1979/80–1994/95. (a) Day -4, (b) day -2, (c) day 0, (d) day $+2$, (e) day $+4$. Contour interval is 10×10^5 m^2 s^{-1}, with negative contours dashed and the zero contour omitted for clarity. Shading denotes OLR anomalies less than -20 W m^{-2}. Locally statistically significant wind vectors are shown, with the largest vectors representing a wind speed about 10 m s^{-1}. Also shown is a portion of a great circle (see text) and a line along 145°W.

associated with anomalously weak jet flow. Opposite anomalies over the eastern North Pacific complete a quadrupole, with the northern branch leading into a weak wave-train pattern over North America and into the North Atlantic. Evidence presented by Meehl et al. (1996) shows that this pattern, and subsequent developments in Fig. 1, are often preceded by equatorial convection in the eastern Indian Ocean at about day -6.

Two days later (Fig. 1b), the jet streak over China has advanced into the jet core, and the trough to its east has shifted eastward and developed a northeast–southwest tilt consistent with the shear deformation zone of positive $\partial u/\partial y$ along the southern margin of the jet. The ridge to its southeast has also developed a stronger positive tilt, while the northern wave train moves more slowly eastward.

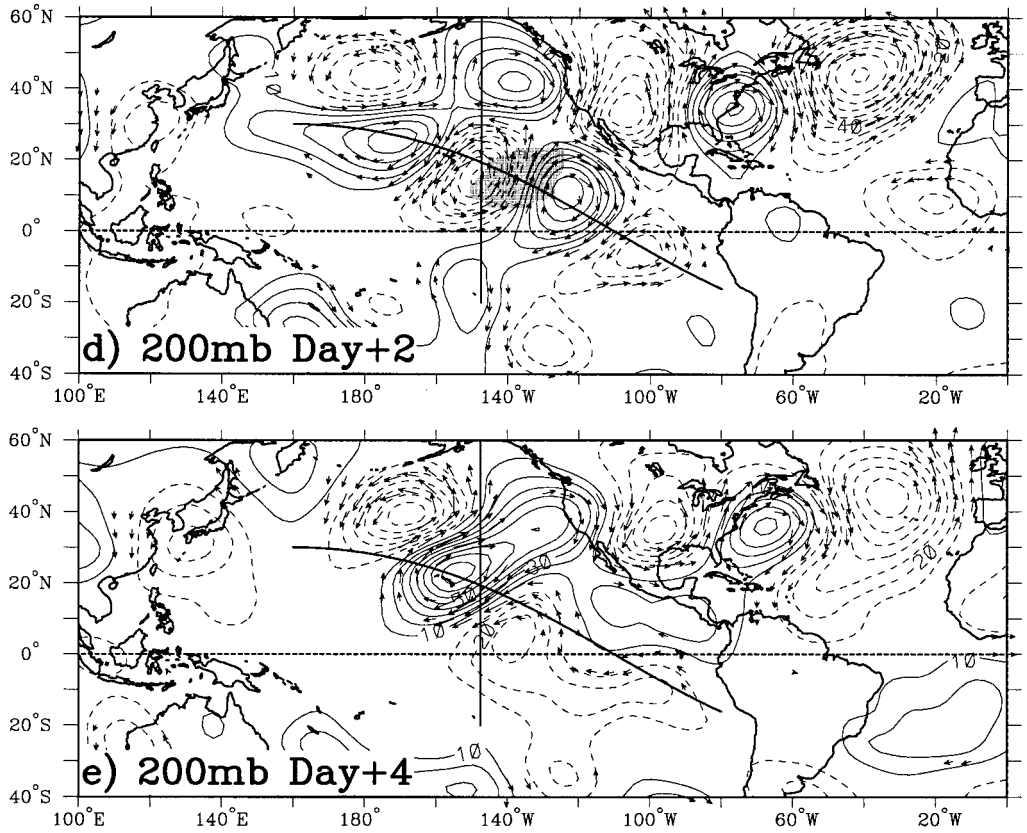

FIG. 1 (*Continued*)

By day 0 (Fig. 1c) the downstream portions of both wave trains have strengthened significantly, while the OLR signal peaks in the ITCZ, ahead of the upper trough located near Hawaii. Group propagation toward the southeast is evident, with clear dispersion apparent as downstream features to the south of the equator are strengthening successively while those upstream weaken. Eastward dispersion along the wave train over North America is also evident. By day +2 (Fig. 1d) the OLR signal has moved eastward and northward, and a substantial circulation has developed just south of the equator near 100°W. Between day −2 and day +4 (Fig. 1e), it is also evident that the pattern has the opposite phase, due to the propagation of features with respect to the earth's surface. This yields a mean period of around 12 days for the disturbance, in agreement with the period derived by Tomas and Webster (1994) and with the spectral results referred to in the previous section.

It is of interest to compare the observed phase and group velocity of the wave train with those for a nondivergent barotropic Rossby wave on a beta plane. Figure 2 is a time–longitude diagram of the streamfunction perturbations along the great circle line in Fig. 1 from day −12 to day +12, within the longitude range 160°E–80°W. This line lies close to the path of the apparent phase and group propagation of the features in Fig. 1, although deviations from this path are observed and to be expected (see below). A phase speed line of 5 m s^{-1} is shown, which approximates the zonal phase speed of individual troughs and ridges within the wave train around day 0, although disturbances within the jet on the left side of the diagram have much faster speeds. Also shown is a 24 m s^{-1} line that gives an estimate of the rate of zonal energy dispersion within the wave train, as shown by the successive development of perturbations farther east over time. This estimate is seen to be most valid for the wave train around day 0, and the next (opposite) phase of the disturbance from days 5 through 10, when the wave energy is crossing the equator.

The approximate spatial scale of the waves can also be estimated from Figs. 1 and 2. From these pictures the wave along the great circle has a zonal wavelength of around 50° longitude, giving a zonal planetary wavenumber of approximately $k = 7$. The meridional wavenumber l at the equator can then be estimated by noting that the angle α that the great circle makes with the longitude–latitude (x–y) coordinate system is

$$\alpha = \tan^{-1}\frac{l}{k}. \tag{1}$$

Since $\alpha = -30°$ at the equator for the great circle shown in Fig. 1, this gives an estimate of around $l = -4$ for the meridional planetary wavenumber at this latitude.

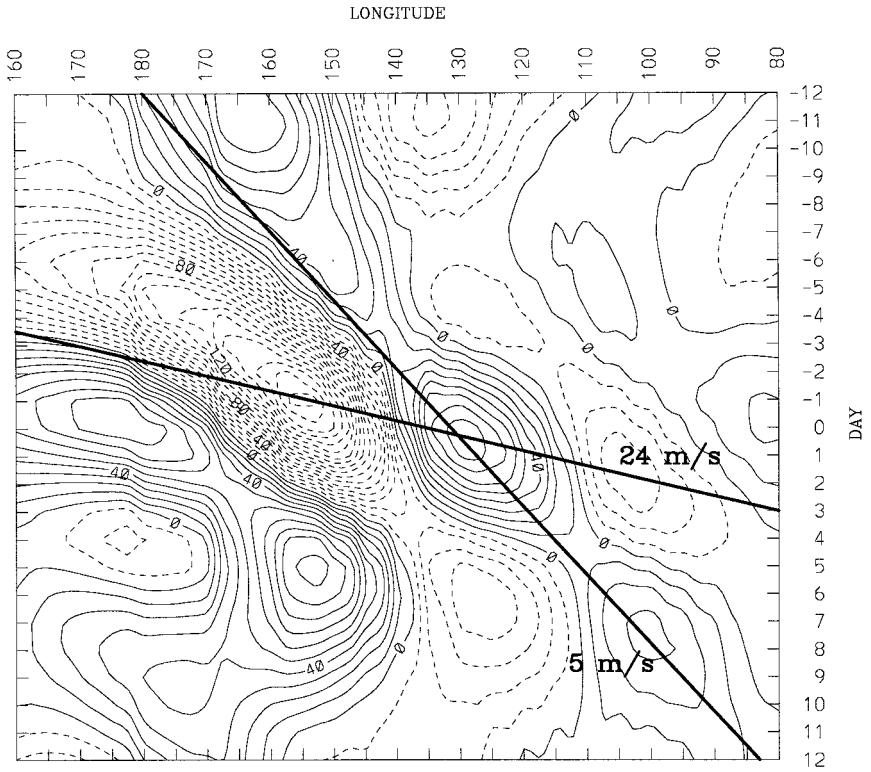

FIG. 2. Time–longitude diagram of 200-mb streamfunction perturbations from day −12 through day +12, along the great circle route shown in Fig. 1. Contour interval is 10×10^5 m^2 s^{-1}, with negative contours dashed. Two phase speed lines of 5 m s^{-1} and 24 m s^{-1} are also shown.

The negative wavenumber is indicative of the positive tilt of the waves in this region.

We will compare the theoretical phase and group velocity with respect to the earth's surface to that of a nonstationary, nondivergent barotropic Rossby wave (e.g., Yang and Hoskins 1996). The dispersion relationship for such a Rossby wave with respect to the earth's surface is given by

$$\nu = \overline{u}k - \frac{\beta k}{k^2 + l^2}, \tag{2}$$

with the zonal phase speed c of

$$c = \nu/k = \overline{u} - \frac{\beta}{k^2 + l^2}, \tag{3}$$

and group velocities u_g and v_g in the zonal and meridional directions, respectively, given by

$$u_g = c + \frac{2\beta k^2}{(k^2 + l^2)^2} \tag{4}$$

$$v_g = \overline{v} + \frac{2\beta kl}{(k^2 + l^2)^2}, \tag{5}$$

where ν is the frequency and $\overline{u}$ is the value of the background zonal wind speed. Setting $\overline{u}$ to zero for the moment, and using the values of β, k, and l at the equator in order to estimate the intrinsic phase and group velocity of such a wave yields $c = -14.3$ m s^{-1}, $u_g = 7.3$ m s^{-1}, and $v_g = -12.3$ m s^{-1}. However, the waves are embedded in a strong background basic state that Doppler shifts these phase and group speeds. Referring to maps of the mean DJF 200-mb flow over the region (e.g., Fig. 1a of Kiladis and Weickmann 1997), we see that along the tropical portion of the ray path in Fig. 1 the zonal flow is nearly constant at about 20 m s^{-1}. Taking $\overline{u} = 20$ m s^{-1} then gives $\nu = 6.3 \times 10^{-6}$ s^{-1}, corresponding to a period of 11.6 days, which agrees well with the mean period of the waves as described above. The zonal phase and group velocity with respect to the ground is then $c = 5.7$ m s^{-1} and $u_g = 27.3$ m s^{-1}, values that match the observed speeds in Fig. 2 reasonably well, considering the gross assumptions made.

If the group velocity were indeed along the great circle route, the observed meridional group speed at the equator would simply be $v_g = u_g \tan\alpha = -13.8$ m s^{-1}, a value that is again not far from that predicted. However, in reality, the ray path for a nonstationary barotropic Rossby wave will deviate from a great circle due to changes in both zonal and meridional advection and refraction by the zonal and meridional gradients in the flow (e.g., Karoly 1983). The meridional flow in the domain of the wave train is certainly not negligible, and moreover, as we shall show, the disturbances are as-

sociated with strong divergence in the region of the ITCZ. Nevertheless, initial value simulations in a barotropic model with a realistic basic state, to be presented elsewhere, do confirm that the observed upper-level waves indeed behave similarly to that predicted by simple Rossby wave theory.

b. 850 mb

Figure 3 shows the evolution of the 850-mb circulation obtained from the identical OLR predictor used to produce Fig. 1. As at 200 mb, the sequence suggests a substantial extratropical influence on ITCZ convection, although the signal is not one of wave energy propagation into the Tropics.

At day -4 in Fig. 3a a large anticyclone is present at 850 mb, which lies beneath the 200-mb anticyclone and subtropical trough at the date line in Fig. 1a. This anticyclone already extends far into the Tropics and is linked to anomalous equatorial easterly flow just to the east of the date line. The collocation of the subtropical portion of this feature with an upper trough is indicative of a negative temperature perturbation in the midtroposphere, discussed in more detail below. To the west is a cyclone over Japan, which shows a pronounced poleward tilt with height. Over North America and the Atlantic, 850-mb signals are for the most part in phase with those at upper levels, although some westward tilt with height is evident, particularly in the feature located near the east coast of North America.

An amplification of the 850-mb anticyclones over the mid-Pacific and North America is seen by day -2, resulting in an increase of the trade wind flow over a broad region of the east Pacific (Fig. 3b). The cyclone off Japan in Fig. 3b moves rapidly northeastward in the Pacific storm track by day 0 (Fig. 3c), at the same time that the Pacific anticyclone surges equatorward and further strengthens the trade wind flow into the region of developing convection. To the west of the convection, a low-level cyclone has formed, with equatorial westerly anomalies coupled to a weak cyclonic feature to the south of the equator. This southern cyclone strengthens significantly by day $+2$ (Fig. 3d) and propagates westward along with the equatorial westerlies over the next couple of days (Fig. 3e).

Throughout the sequence of Figs. 1 and 3 the evolution of the extratropical features are characteristic of baroclinic wave development, where westward and poleward tilts with height are evident near Japan and the southeastern coast of North America, becoming more equivalent barotropic as the disturbances move northeastward into the storm tracks over the Pacific and Atlantic. The low-latitude vertical structure is more complicated, with like-signed wind perturbations in some regions, such as along the equator near 160°W on day 0, as opposed to very weak perturbations at low levels beneath strong signals at 200 mb over the east Pacific.

The pattern of westward-propagating paired cyclonic anomalies along the equator at 850 mb in Fig. 3 is characteristic of the $n = 1$ equatorial Rossby waves isolated in the 6–30-day band by Kiladis and Wheeler (1995). The equivalent barotropic vertical structure, with like-signed wind anomalies through a deep layer of the troposphere near the equator and convection in the poleward flow to the east, is also consistent with our observations of those modes. One interpretation of this analysis is that low-level equatorial Rossby waves may be initiated by upper-level wave activity from the extratropics, as has been suggested for the generation of mixed–Rossby gravity waves (e.g., Zhang and Webster 1992; Magaña and Yanai 1995). However, the role of ITCZ convection as an energy source is still an open question, and resolution of these issues will likely require additional theoretical and modelling work, as discussed further in section 6.

c. Mass circulation

The OLR signal in Figs. 1 and 3 is accompanied by a substantial mass circulation at 200 mb, as shown in Fig. 4. In Fig. 4a a region of perturbation divergence is almost perfectly collocated with the negative OLR signal, with a wave train of divergence anomalies in quadrature with the streamfunction anomalies of Fig. 1. This relationship gives us confidence that at least the qualitative pattern, if not the exact magnitude, of the divergence field is well-captured by the NCEP reanalysis data, since OLR is virtually independent of the analysis. The divergent wind (Fig. 4b) shows rather large-scale upper-level outflow away from the convective region, which is stronger toward the winter hemisphere but also crosses the equator into the eastern South Pacific convergence zone (SPCZ) region. A sharply defined line of convergence is found at the junction between the tropical outflow and divergent outflow from the storm track cyclone farther northwest. The strength of the tropical divergent circulation is substantially larger than that observed for the mean circulation in this region (e.g., Mo and Rasmusson 1993); thus these transient events are likely important for the vorticity balance of this region.

At 850 mb, convergence into the convective region yields a pattern qualitatively opposite to that observed in Figs. 4a and 4b (not shown). This implies upward motion in the negative OLR region, which must then peak somewhere in the midtroposphere, a structure which is verified in section 4.

d. Isentropic potential vorticity

In the case study examined by Kiladis and Weickmann (1992b), an upper-level trough at low latitudes was shown to be accompanied by a strong signal of equatorward propagating high isentropic potential vorticity (IPV) air on the 350-K potential temperature (θ)

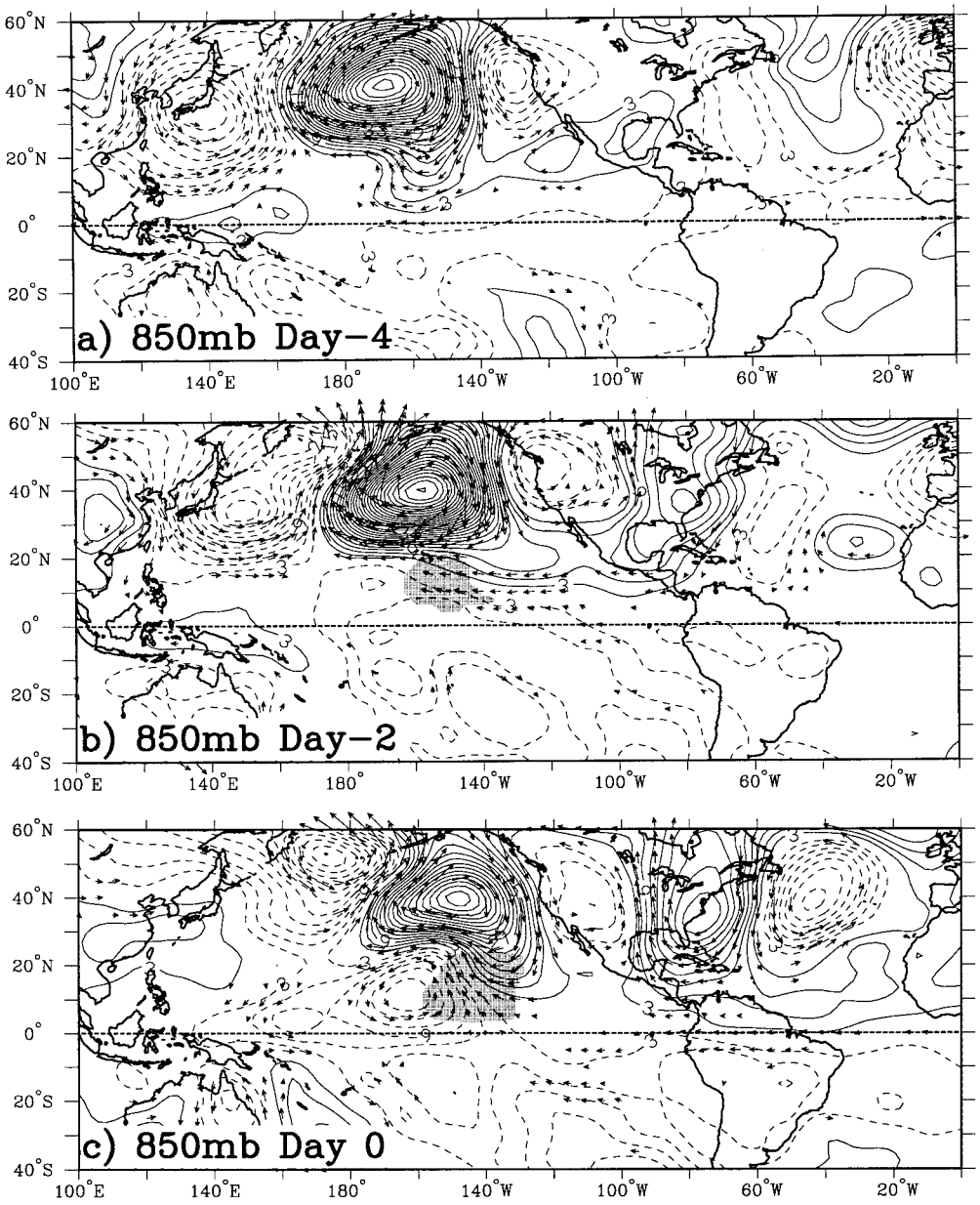

FIG. 3. As in Fig. 1, except for 850-mb streamfunction perturbations. Contour interval is 3×10^5 m^2 s^{-1}. The largest vectors are about 3 m s^{-1}.

surface (see Hoskins et al. 1985). A negative OLR anomaly in the ITCZ was located ahead of this IPV anomaly, in a region of strong positive PV advection, where upward motion should be maximized.

Figure 4c maps the regressed horizontal distribution of IPV on the 350-K surface at day 0 corresponding to the streamfunction pattern in Fig. 1c. This θ surface lies close to the 200-mb pressure level at all latitudes. The IPV distribution was computed by adding the regressed wind and temperature fields using the OLR predictor to those corresponding to the DJF mean at the appropriate pressure levels. These values of PV were then interpolated to the 350-K surface and mapped in ''PV units'' ($=1 \times 10^6$ m^2 s^{-1} K kg^{-1}).

A positively tilted ''trough'' of high PV air is present immediately northwest of the OLR anomaly in Fig. 4c. Lagged maps (not shown) depict this signal originating as a small ripple propagating eastward within the strong PV gradient along the Asian jet a few days prior to day 0, followed by a rapid amplification and equatorward propagation from the jet exit region into the Tropics. This evolution matches that of the case studied by Kiladis and Weickmann (1992b) quite closely, although in individual events the PV ridge will typically be much

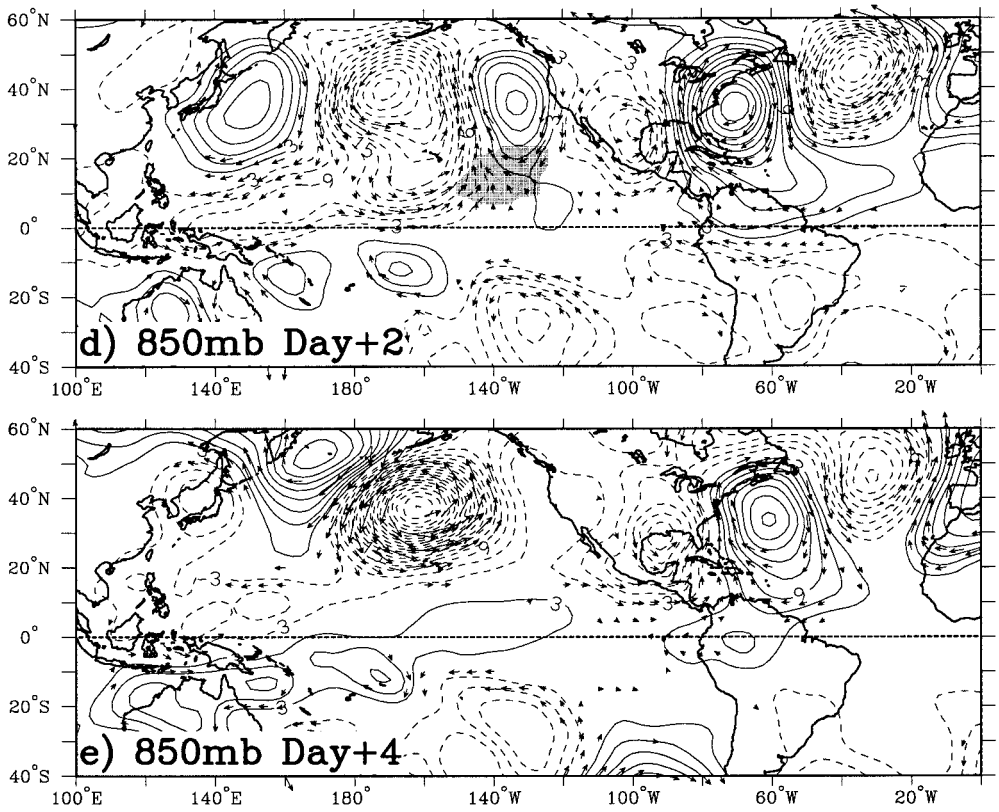

FIG. 3. (*Continued*)

more narrow and sharper than the feature in Fig. 4c, due to the ''smearing'' from the noise inherent in the regressions. It is also notable that the negative streamfunction perturbation near the equator, 100°W in Fig. 1c, is associated with another trough of positive PV crossing into the Southern Hemisphere in Fig. 4c.

In lagged maps of IPV perturbations (not shown) the positive IPV anomaly present to the northwest of the OLR anomaly weakens considerably by day +2 as it moves eastward. This weakening can occur through the advection and consequent flux divergence (or ''rearrangement'') of PV along θ surfaces by barotropic processes, or by diabatic effects that transport mass across θ surfaces and effectively ''dilute'' the PV (Haynes and McIntyre 1987). The former is unlikely to be the dominant process here, since the PV appears not so much ''spread out'' over time but disappears very rapidly more or less in situ. Most likely the diabatic heating associated with the convection is primarily responsible for this evolution; however, quantification of this effect through a PV budget analyses, and modeling, will be necessary to confirm this.

4. Vertical structure

a. Potential vorticity

Tomas and Webster (1994) examined the vertical structure of equatorward propagating disturbances in the eastern Pacific during northern winter by correlating PV at 200 mb to that at standard pressure levels from 1000 to 100 mb in the vertical. Their analysis showed that the waves propagated freely across the equator in the upper-level westerlies, but at lower levels only weak signals penetrated into the trade winds. Thus, the vertical extent of the waves was seen to become more shallow as lower latitudes were approached. It was speculated that the zero zonal wind line acted as a critical line in the vertical, such that the wave activity was precluded from propagating from the upper westerlies into the low-level easterlies.

Here we take a somewhat different approach by using OLR as the independent variable and examining the actual regressed values of PV on pressure surfaces. Vertical cross sections of the evolution of PV on the 14 standard pressure levels were produced in the zonal and meridional directions, as well as along the great circle route shown in Fig. 1. Since the regression analysis allows the relative amplitude of a given parameter at each level to be preserved, a detailed view of the typical vertical distribution of PV associated with ITCZ convection can be depicted.

Figure 5a shows the day 0 distribution of PV perturbations on pressure surfaces in the zonal direction along 10°N. Since lower tropospheric PV is so small near the equator, the contour interval has been reduced

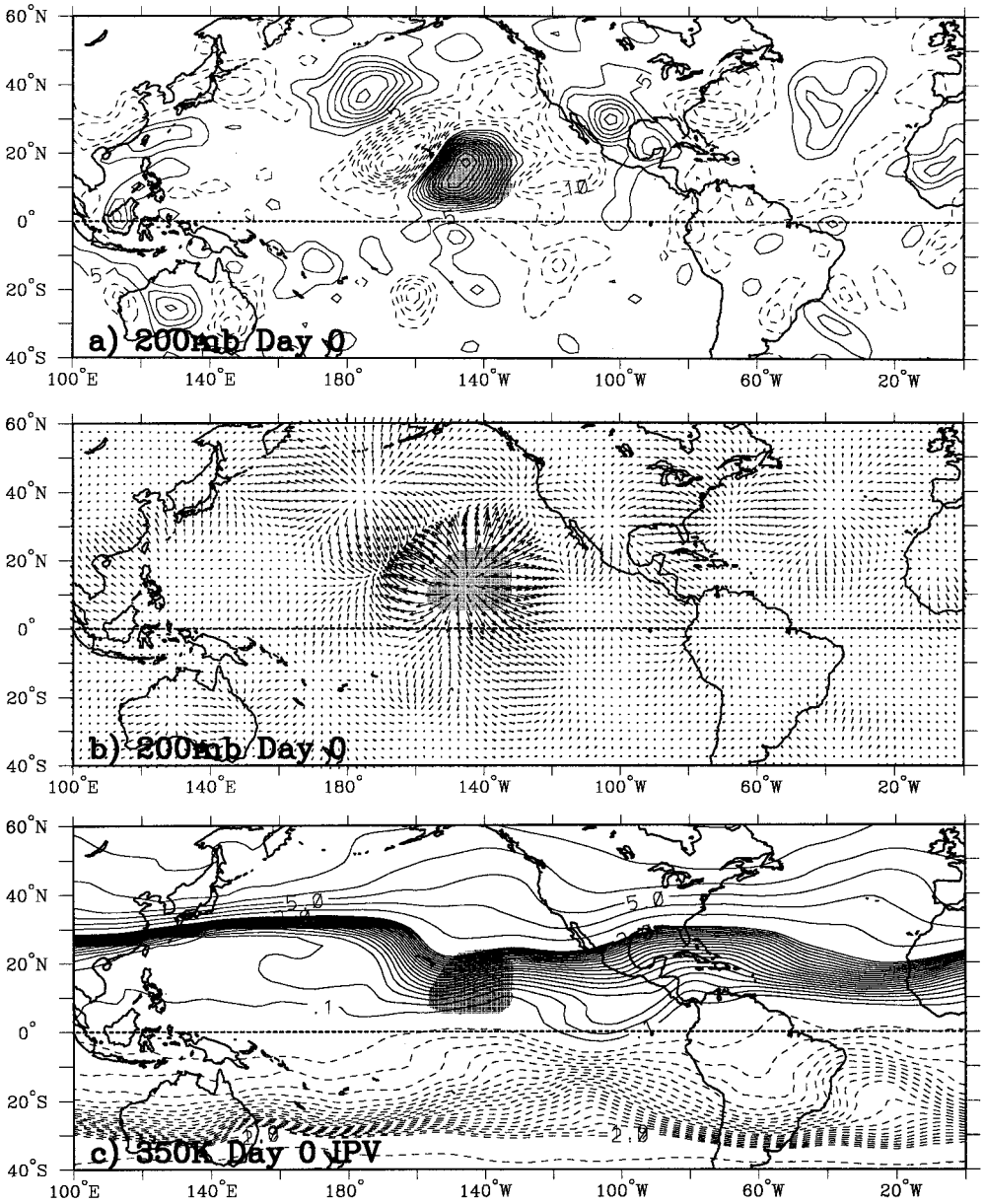

FIG. 4. As in Fig. 1, except for (a) day 0 200-mb divergence. Contour interval is 5×10^{-7} s^{-1}. (b) Day 0 200-mb divergent wind. Largest vectors are around 2 m s^{-1} magnitude. (c) Day 0 isentropic potential vorticity on the 350-K surface, in PV units ($=1 \times 10^{6}$ m^2 s^{-1} K kg^{-1}). Contour interval is 0.1 PV units between -2.0 and $+2.0$, and 1 PV unit otherwise.

to 0.02 PV units for values less than 0.14 in this figure, and 0.10 otherwise. The largest PV anomalies at this latitude are in the lower stratosphere, with the location of the OLR signal, at 145°W, in between the largest tropospheric PV anomalies. There is a pronounced westward tilt with height of the stratospheric signals, and weaker but opposite tilts below about 100 mb.

The total PV on day 0 and day +2 in Figs. 5b and 5c is obtained by adding the DJF mean state for the study period to the perturbations. The waves are represented by vertical undulations in the pressure level of PV, which progress eastward over time. In Fig. 5b two marked downward excursions of the contours represent the anomalously high PV in the mid and lower troposphere to the west and east of the convection, as was also seen in Fig. 4c. Also notable is the 0.2 contour of PV below 700 mb centered at the date line, which represents the cyclonic circulation at 850 mb in Fig. 3c. While this lower signal is initially vertically aligned with the midtropospheric anomaly in previous lags (not shown), over time it drifts westward and becomes detached from the eastward-moving upper anomaly.

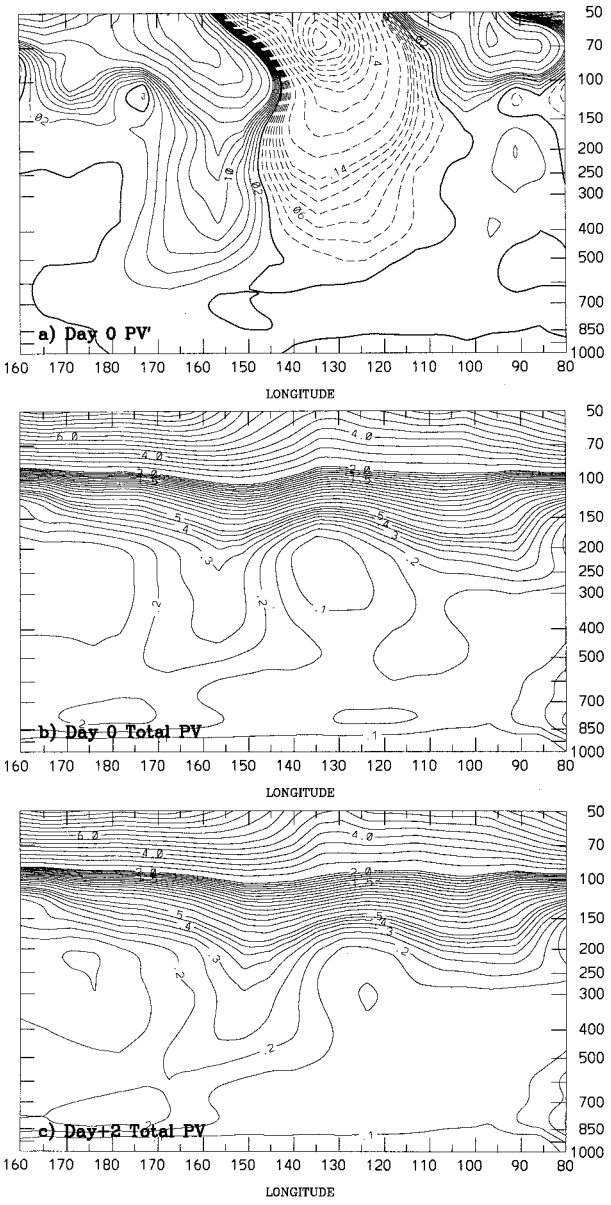

FIG. 5. Vertical cross sections in the zonal direction at 10°N of (a) day 0 perturbation PV. Contour interval is 0.02 PV units between −1.4 and +1.4, 1.0 otherwise. (b) Day 0 total PV. (c) Day +2 total PV. Contour interval in (b) and (c) is 0.05 PV units from 0.1 to 0.5, 0.1 units from 0.5 to 2.0, and 0.5 units otherwise.

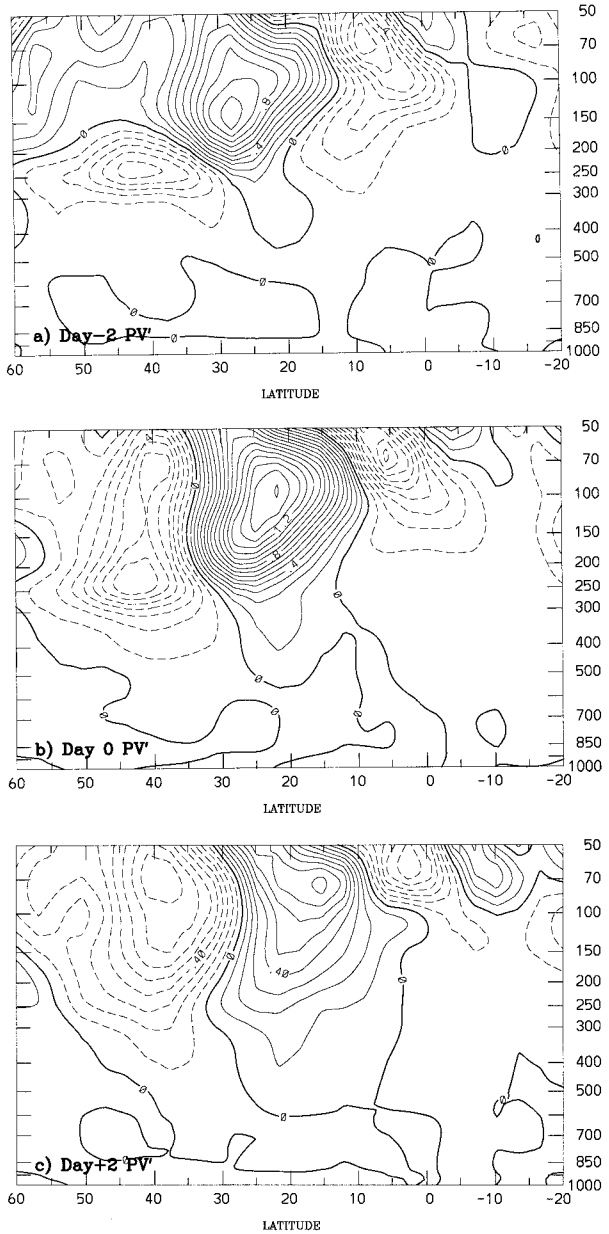

FIG. 6. As in Fig. 5, except for in the meridional direction along 145°W (along the vertical lines in Figs. 1 and 3). (a) Day −2. (b) Day 0. (c) Day +2. Contour interval is 0.1 PV units.

Figure 6 shows the evolution, from day −2 to day +2, of PV anomalies on pressure surfaces in the meridional plane along 145°W (marked by the vertical line in Figs. 1 and 3), which passes through the region of maximum OLR perturbation. These sections are similar to those along the great circle (not shown). Pronounced poleward tilts of the waves are seen in the stratosphere, and as in the zonal direction there are weaker but opposite tilts below 100 mb. Another feature evident in Fig. 6, besides the equatorward progression of the anomalies, is their apparent vertical propagation into the stratosphere, consistent with their poleward and westward tilts with height above the 100-mb level.

As the PV anomalies move equatorward they become more vertically constrained, in agreement with the Prandtl–Rossby–Burger relationship,

$$H \sim fL/N, \tag{6}$$

where H is the vertical scale, L is the characteristic horizontal scale, and N is the Brunt–Väisälä frequency [see also Eq. (33b) in Hoskins et al. 1985]. This relationship shows that the depth of influence of a PV per-

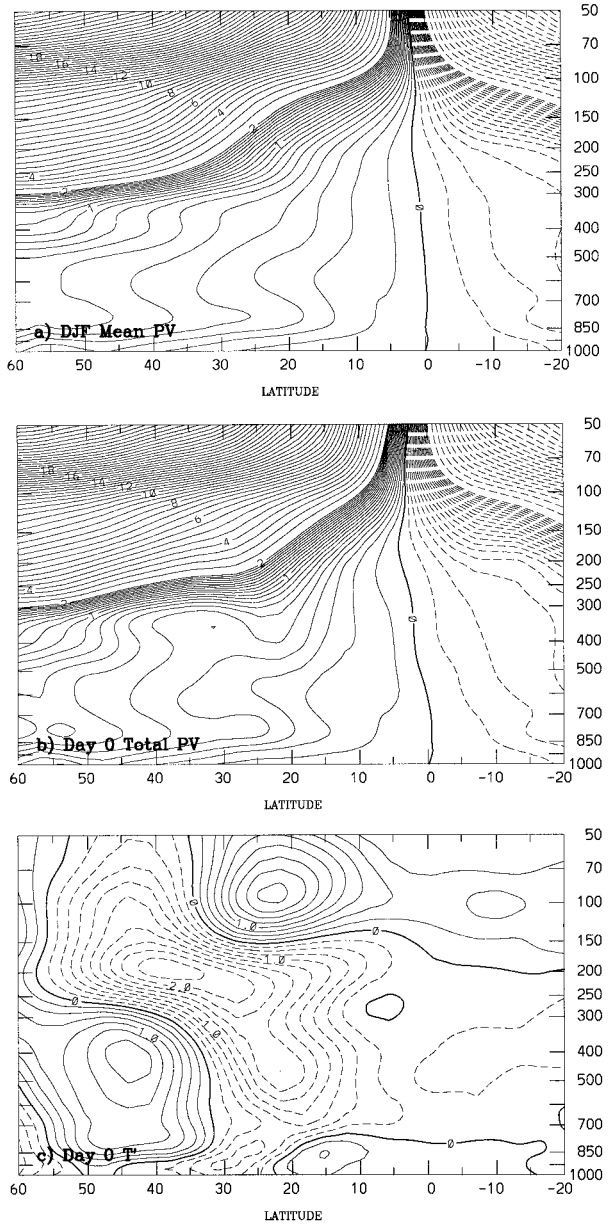

FIG. 7. As in Fig. 6, except for (a) DJF 1979/80–1994/95 mean PV along 145°W. (b) Day 0 total PV. Contour interval in (a) and (b) is 0.1 PV unit between −2.0 and +2.0, 0.5 units otherwise. (c) Day 0 temperature anomaly along 145°W. Contour interval is 0.25 K.

turbation should decrease both as the perturbation moves equatorward (f decreasing) and as it propagates vertically (increasing N), as seen in Fig. 6.

One way to understand the apparent upward propagation of the disturbances in a qualitative sense is by considering the vertical orientation of the PV field in the meridional direction. Figure 7a shows the climatological distribution of total PV along the meridional cross section. The PV contours in these plots (as in the zonal mean) are quasi-horizontal poleward of 30°N and increasingly sloped to the south, to become nearly vertical at the equator. In the midlatitudes the tropopause generally lies around the 1.5-PV unit level. Clearly at low latitudes, however, this contour must cut across the tropopause, which is at around 100 mb at the equator. The strong, vertically sloping PV gradient can act as a wave guide to sufficiently large perturbations along it (Hoskins et al. 1985), leading to the upward propagation of wave activity. The effect of the day 0 PV perturbation on the total field is shown in Fig. 7b, where the downward excursion of contours is evident at 20°N. The ''bulges'' associated with the wave activity progress equatorward and upward along the strong gradient over time (not shown), with the waves subtly altering the vertical orientation of the PV distribution near the equator, as can be seen by comparing Figs. 7a and 7b.

b. Temperature

A deep layer of cold air advection accompanies the upper PV anomaly and associated trough, which was also a prominent feature of the case study in Kiladis and Weickmann (1992b). A meridional section (Fig. 7c) shows the largest negative temperature perturbation exceeding 2 K; it peaks at 250 mb poleward of 30°N and extends downward into the subtropics and Tropics, crossing the equator. There is a warm anomaly at the surface and in the stratosphere in the Tropics. The net effect of this temperature distribution is to make the lower troposphere less stable at low latitudes, as shown by the change in $\partial T/\partial p$, which has a local maximum near the 700-mb level at about 15°N (not shown).

c. Vertical motion

The combination of dynamical forcing by positive PV advection at upper levels and decreased stability at low levels due to temperature advection is to induce upward motion along the ITCZ. Figure 8a shows the mean DJF 1979/80–1994/95 vertical distribution of ω ($=dp/dt$) along the 145°W reference line. Also shown is a representation of the mass circulation in the meridional plane, obtained by combining the divergent meridional wind and ω, and scaling the arrows such that a 1 m s^{-1} meridional divergent wind is equal to a 5×10^{-2} Pa s^{-1} vertical motion. The ITCZ is well defined in the reanalysis data, with mean upward motion between 2.5°N and 10°N, peaking at 7.5°N. Mean tropospheric subsidence at the equator is in agreement with profiler observations at Christmas Island, 12° of longitude farther west (Gage et al. 1991). The SPCZ is also seen as a broad region of negative ω to the south of the equator, as is the storm track poleward of 40°N. Most of the subtropical subsidence in the Northern Hemisphere subtropics is confined to the lowest levels at this longitude, as opposed to zonal mean conditions (not shown), where it is maximized at around 400 mb.

Figure 8b shows the sum of the mean state from Fig. 8a and the perturbation ω field, scaled once again to a

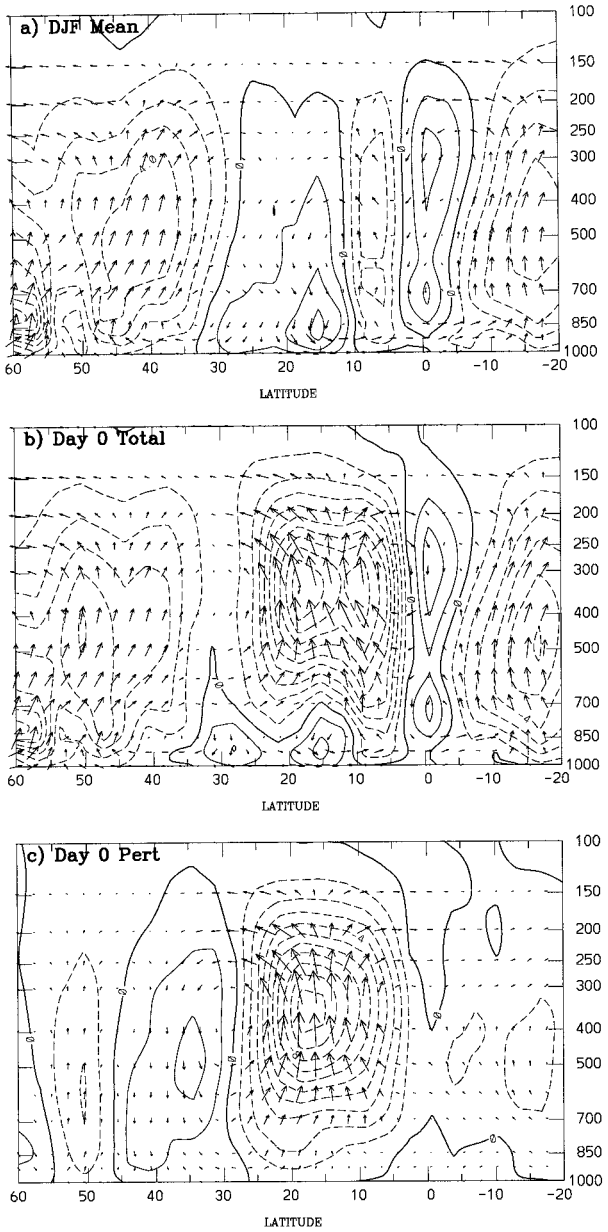

FIG. 8. As in Fig. 7, except for ω ($=dp/dt$), shown by the contours, and the mass circulation shown by the vectors. The contour interval is 1×10^{-2} Pa s^{-1}, and the vectors are scaled such that a 1 m s^{-1} meridional divergent wind is equal to a -5×10^{-2} Pa s^{-1} vertical motion. (a) DJF 1979/80–1994/95 mean. (b) Day 0 total ω. (c) Day 0 perturbation ω.

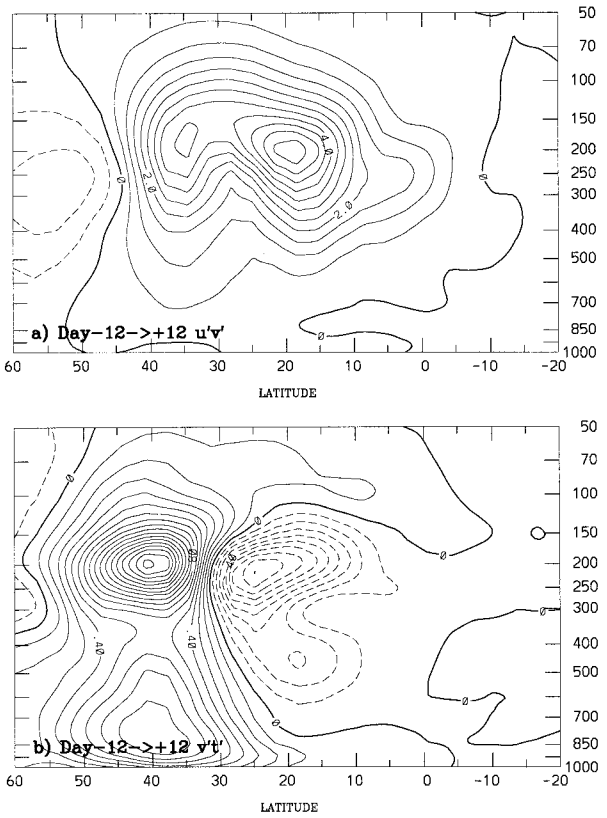

FIG. 9. As in Fig. 8, except for the average from day -12 to day $+12$ and over the longitude range 160°E–100°W of (a) $u'v'$, contour interval is 0.5 m^2 s^{-2}; (b) $v'T'$, contour interval is 0.1 m K s^{-1}.

-40 W m^{-2} OLR anomaly. Upward motion is greatly enhanced from the ITCZ northward to beyond 20°N. The wave forcing concentrates a vertical velocity maximum at about the 300-mb level at 20°N, with a secondary maximum at the latitude of the ITCZ itself. Interestingly, there is still downward motion below 700 mb centered on 15°N. There is also little change in the mass circulation away from the northern subtropics, although the perturbation field in Fig. 8c shows that a weak region of subsidence completes an anomalous local Hadley circulation extending out to about 40°N. The magnitude of this horizontal divergent circulation (see also Fig. 4b) is certainly large enough to produce a substantial vorticity tendency at upper levels of the subtropics. The quantification of this tendency and its effect on the evolution of the subtropical westerlies and associated cloud band will be explored in a future study.

d. Momentum and heat transports

A view of the of the meridional transport of westerly momentum in the region of the wave train is shown in Fig. 9a. This was obtained by calculating the daily product $u'v'$ at each grid point and pressure level from day -12 to day $+12$ from the regressed fields. These products were then averaged over the day -12 to day $+12$ cycle and also over the longitude range 160°E to 100°W, which encompasses the domain of the wave train in the zonal direction. This 25-day averaging procedure covers two ''cycles'' of the mean period of the wave and is meant to give a qualitative picture of the vertical distribution of poleward momentum flux associated with the disturbances. Since this calculation includes only products between separately filtered and regressed 6–30-day u' and v', and not cross products that would be

associated with interactions between this band and other frequencies, it comprises only a portion of the impact of these transients on the momentum budget, although calculations of these other quantities (not shown) show negligible contributions.

As expected from the positive tilt of the wave train in Fig. 1, there is a poleward flux of westerly momentum extending from just south of the equator to 50°N associated with the cycle, which peaks at around the 200-mb level. The primary maximum of poleward flux at 20°N suggests an acceleration of the westerlies at around 30°N, and a flux divergence and deceleration of the westerlies in the deep Tropics. Thus the propagation of this type of wave activity into the westerly duct acts as a brake on the equatorial westerlies themselves.

The calculation of $v'T'$ by the same method (Fig. 9b) shows two peaks in the poleward flux of heat at 40°N in the lower and upper troposphere, with positive values extending to just south of the equator below 850 mb and in the stratosphere. Despite the cold advection present near the convective region on day 0, the net effect of the wave activity results in equatorward (poleward) movement of warm (cold) air in the mid- to upper levels of the subtropics. This countergradient heat flux is typical of the climatological transient eddy statistics at this time of year (e.g., Newell et al. 1974) and is also consistent with the vertical tilts of the eddies at low latitudes in Fig. 5 (e.g., Hoskins et al. 1983), where upward (downward) group propagation is associated with a poleward (equatorward) heat flux in the stratosphere (troposphere).

5. Equatorward propagating wave activity and the general circulation

a. Mean conditions

As discussed in section 1, positively tilted, equatorward-propagating transients at low latitudes are a necessary feature of the momentum balance of the general circulation. During northern winter these transients over the eastern Pacific, North America, and Atlantic region play a crucial role by transporting westerly momentum poleward. One convenient way of examining the time-mean signal of these transients on the mean circulation is through the *E* vector representation of Hoskins et al. (1983). The horizontal *E* vector is a pseudo-vector constructed by calculating time-mean covariances between the perturbation zonal and meridional wind components:

$$\mathbf{E} = (\overline{v'^2 - u'^2}, \overline{-u'v'}). \tag{7}$$

The term $\overline{v'^2 - u'^2}$ is a measure of the mean anisotropy or shape of the waves. For example, if v'^2 is consistently larger than u'^2, the waves are preferentially elongated in the meridional direction and the *E* vector points eastward, as is the case for high-frequency (<10 day) intraseasonal fluctuations at the Asian jet exit region (Hoskins et al. 1983; Wallace and Lau 1985). The *y*-component $\overline{-u'v'}$ is minus the time–mean northward flux of westerly momentum associated with the perturbations. Together the two components approximate the preferred direction of the group velocity of the waves using suitable approximations, including the assumption of quasigeostrophy.

Kiladis and Feldstein (1994) showed that the east Pacific Rossby wave activity propagating into the Tropics dominated the less than 14-day *E* vector field in that region for DJF 1979/80–1989/90 NCEP operational analyses at 200 mb. Here we perform a similar calculation for 6–30-day transients using the 1979/80 through 1994/95 NCEP reanalysis data.

Another useful diagnostic for representing the mean background state in which the transients are embedded involves the calculation of the stationary Rossby wavenumber:

$$K_s = \left(\frac{\beta_*}{\overline{U}}\right)^{1/2}, \tag{8}$$

where

$$\beta_* = \beta - \frac{\partial^2 \overline{U}}{\partial y^2}$$

is the meridional gradient of absolute vorticity associated with the basic state. Here, K_s is the total wavenumber at which a barotropic Rossby wave is stationary at a particular location in a given background zonal flow. Karoly and Hoskins (1982) and Hoskins and Ambrizzi (1993) show that the distribution of K_s can be used to infer the location of critical lines and wave guides for stationary Rossby waves, again subject to some approximations. Although the waves studied here are clearly not stationary, Yang and Hoskins (1996) show that a modified *K* for transient waves can still give useful information on the dependence of nonstationary eddy activity on the background state. Here we will use K_s to give a qualitative picture of the effects of the basic-state flow within the westerly duct on the equatorward wave propagation.

Figure 10a shows the 6–30-day mean 200-mb DJF *E* vector field over the Pacific domain for 1979/80–1994/95, along with a calculation of K_s for the same period. The imprint of the equatorward-propagating wave activity is evident as a large region of southeastward-pointing *E* vectors that extends from the Asian jet exit region near the dateline into central North America. These eddies reach farthest into the Tropics from about the dateline to around 120°W, matching the longitude range of maximum correlation between OLR and upper level wave activity (Kiladis and Weickmann 1992b, 1997). A small region of zonally oriented eddies in the Asian jet core gives way to meridionally elongated signatures to the east and south. The transients again become more zonally elongated at about 10°N, where the *E* vectors begin to point southwestward. There is a notable lack of *E* vector amplitude near the critical line

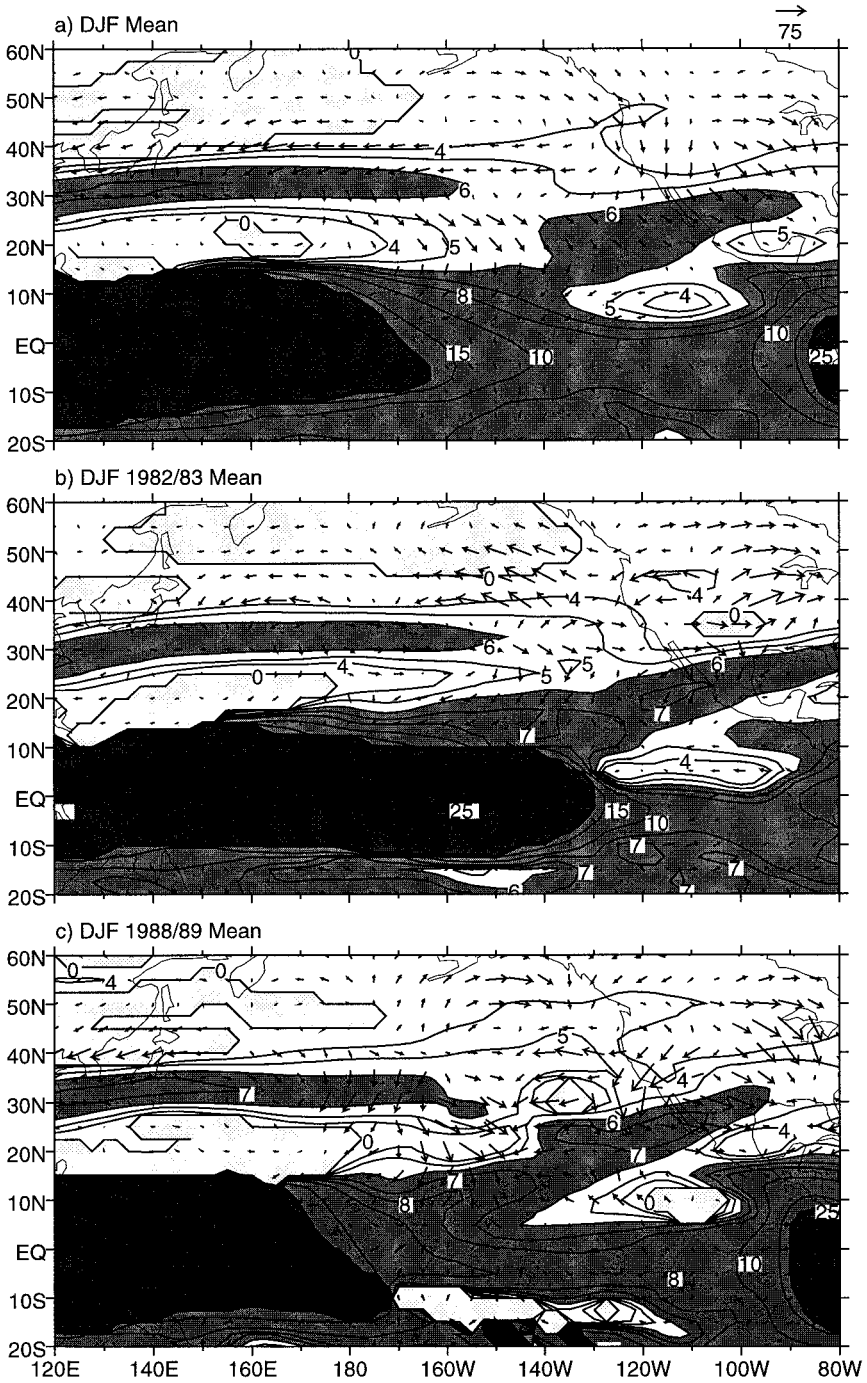

FIG. 10. 200-mb E vectors and K_s (see text) for (a) DJF 1979/80–1994/95 mean. (b) DJF 1982/83, and (c) DJF 1988/89. Contours appear at zonal wavenumbers 0, 4, 5, 6, 7, 8, 10, and 15, and a heavy contour at 25 represents the transition to regions of easterly zonal wind and imaginary K_s. Light shading shows regions of negative absolute vorticity gradient; medium shading regions between zonal wavenumbers 6 and 25, and heavy shading regions of easterly zonal wind. The largest vectors are around 100 $m^2\ s^{-2}$.

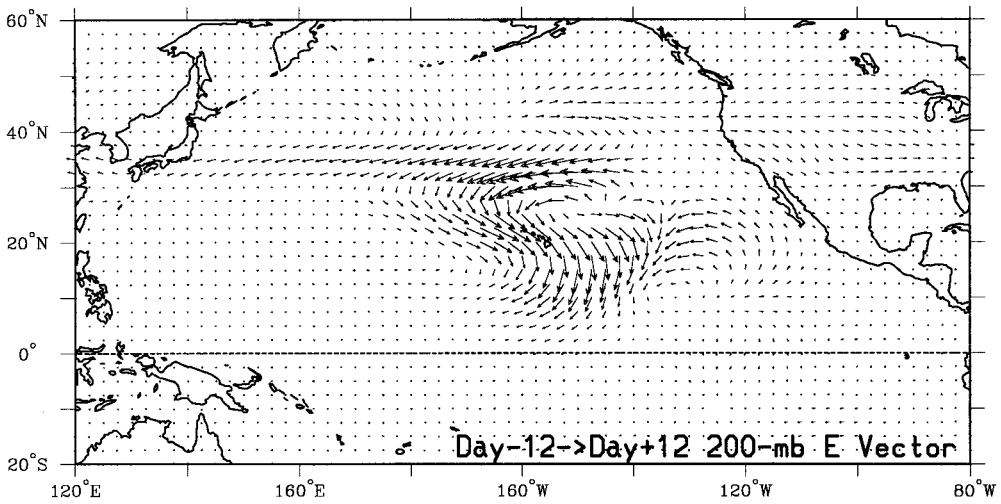

FIG. 11. Mean 200-mb E vectors from day -12 to day $+12$. Largest vectors are around 100 m^2 s^{-2}.

region of the tropical west Pacific, as shown by the thick contour where K_s approaches infinity ($\overline{U} = 0$). Consistent with refractive index considerations, the E vectors tend to point across the gradient and toward regions of higher K_s, such as toward the ITCZ south of Hawaii, and avoid regions of local K_s minima, as near 10°N in the easternmost Pacific and south of the Asian jet.

Hoskins et al. (1983) show that a convergence of E vectors implies that the transient eddies are acting to decelerate the background zonal wind. This occurs along the northern edge of the central Pacific ITCZ and eastward into southern North America in Fig. 10a. Kiladis and Feldstein (1994) calculated the DJF zonal momentum budget over the eastern tropical Pacific at 200 mb from NCEP operational analyses and found that the transient eddy terms were indeed crucial to the budget and acted to decelerate the westerlies over that region. This budget was recalculated using 1979–95 reanalysis data, and again a good balance was obtained, with the residuals in most locations less than 20% of any one term in the budget (not shown). Filtering reveals that most of this transient eddy deceleration of the zonal wind occurs on timescales of less than 30 days.

b. *E vector signal of wave activity associated with ITCZ convection*

The 200-mb E vector signature of the 6–30-day wave activity is mapped in Fig. 11, calculated in the same way as the covariance terms in Fig. 9 over the 25-day cycle of lagged regressions. The mean E vectors of the wave activity have a signature similar to the time mean DJF picture in Fig. 10a, with zonally elongated eddies in the Asian jet, meridionally elongated and southeastward-propagating transients to the south of the jet exit region, and E vectors turning southwestward at around 10°N. The poleward flux of westerly momentum, which is maximized at this level in Fig. 9b, and the convergence of E to the north of the ITCZ, are also reflected in the mean picture. One notable difference is that the transients we have isolated as being associated with convection at 145°W remain zonally elongated past the dateline, as can be seen in Fig. 1. Of course, these disturbances contribute to only a portion of the climatological transient eddy effects, although it appears that they are the dominant features leading to the climatological E-vector picture over the study region in Fig. 10a.

c. *Interannual variability of wave activity*

An example of the interannual variability in the east Pacific wave activity can be obtained by referring to Figs. 10b and 10c, which show the 6–30-day 200-mb E vectors and K_s for two individual DJF seasons, 1982/83 and 1988/89. The time–mean zonal wind contributing to Fig. 10b differs substantially from the mean picture in Fig. 10a due to the extreme warm event conditions associated with unusually high sea surface temperature (SST) and eastward and equatorward expansion of convection over the eastern equatorial Pacific during that period (e.g., Gill and Rasmusson 1983). The eastward shift of the critical line compared to climatology is evident during that season, which is directly related to the establishment of upper-level easterlies and the breakdown of the westerly duct as a response to the anomalous convection. The E-vector signal shows a marked reduction in its normal amplitude to the south of 20°N and a northward shift in the latitude where the vectors turn southeastward and the eddies become zonally elongated. This reduction in low-latitude Rossby wave propagation is in agreement with the observation of McGuirk et al. (1987) and Iskenderian (1995) that, despite the extremely active convection along the equator during that season, the 1982/83 winter had little cloud band activity. Thus the equatorial ITCZ convec-

tion during warm events behaves more like the usual warm pool convection over the west Pacific, which is forced by high SST rather than lateral forcing from waves originating in the extratropics.

As a contrast, Fig. 10c shows the same calculations for the DJF 1988/89 cold event season. In this case SST was much below normal over a large portion of the tropical east Pacific, and the upper-level westerlies were stronger than normal in the westerly duct. As a result the critical line is west of its mean position and the wave activity is also shifted south and west, with higher amplitude when compared to climatology. A large region of low OLR was observed around 15°–20°N, 140°–120°W, well north of the mean ITCZ location (Arkin 1989), despite the fact that the SST was below normal throughout this region during the period. This is where there is strong anomalous convergence of *E* vectors in Fig. 10c, suggesting that increased wave activity into the westerly duct was responsible for forcing this northward shift in the ITCZ along with enhanced cloud band activity.

6. Discussion

The findings of this study may be summarized as follows.

1) *Equatorward propagating Rossby wave activity in the eastern tropical Pacific during northern winter appears to modulate cloudiness, stability, and vertical motion in the vicinity of the ITCZ.*

There is strong evidence that the wave activity can trigger convection within the ITCZ through the dynamical effects of potential vorticity advection into low latitudes. Upward motion induced ahead of high values of IPV intruding into the deep Tropics appears to trigger tropical convection through vorticity advection and the associated decrease of static stability at low levels.

2) *The horizontal propagation of the wave activity in the upper troposphere and lower stratosphere behaves approximately like a nondivergent barotropic Rossby wave.*

The wave activity has maximum amplitude at around the tropopause level in the subtropics. Despite their likely association with convection at times, both the phase and group propagation are roughly comparable with that expected for a nondivergent barotropic Rossby wave with a spatial scale and horizontal tilt similar to that observed. Although the waves are propagating through a basic state with strong horizontal and vertical shears, the *E*-vector signatures of the wave activity are consistent with the inferred refractive index properties of this flow, as shown in section 5. Ray tracing and barotropic modeling may be useful to further illuminate the behavior of the waves, as far as can be explained by linear Rossby wave theory.

3) *The wave activity becomes more vertically constrained and propagates into the stratosphere as it moves equatorward through the subtropics.*

The vertical shrinking and propagation into the stratosphere of the waves as they approach low latitudes is a robust feature of these disturbances. The westward tilt with height and upward propagation is reminiscent of the life cycle of idealized baroclinic waves along a jet modeled by Thorncroft et al. (1993), where a trailing low-latitude region of high PV air propagates equatorward and upward during the later stages of development.

4) *Paired cyclonic disturbances propagate westward along the equator at low levels to the west of the upper-level wave activity and ITCZ convection.*

The signature of westward propagating symmetric perturbations on either side of the equator, with off-equatorial convection occurring in the low-level poleward flow, is similar to the signature identified in observations by Kiladis and Wheeler (1995) as the equatorially trapped $n = 1$ Rossby mode of shallow water theory.

5) *The wave activity appears to be an important component of the momentum balance in the tropical eastern Pacific region.*

The equatorward-propagating waves identified in this study are likely responsible for the bulk of the upper-tropospheric transient eddy activity over the eastern tropical Pacific during northern winter, as shown through *E*-vector diagnostics in section 5. These positively tilted transients act as a brake on the equatorial westerlies, which are in turn accelerated by the fluxes associated with the time–mean flow (see Kiladis and Feldstein 1994).

6) *There is substantial interannual variability of the wave activity.*

There is large interannual variability of seasonal mean *E* vectors, as well as in the cloud band signatures associated with the wave activity. This suggests that the wave activity is sensitive to alterations in the large-scale basic-state circulation and reorganization of transient activity accompanying such basic-state changes.

Various satellite estimates of ITCZ precipitation show a local maximum around 140°W during DJF (Janowiak et al. 1995), coinciding with the region of maximum wave activity at this time of the year. It seems plausible that this rainfall maximum might be a result of the preferred path of the wave activity (see Fig. 10a), since it is obvious from the OLR signals isolated in the present study that high-level cloudiness is enhanced when upper-level troughs intrude into the region. The quantification of the effect of the wave activity on the variability of ITCZ rainfall itself needs to be established.

Upward propagation of the wave activity is consistent with wave guiding by the vertically sloped tropopause and associated PV contours at low latitudes. It is also in agreement with the vertical distribution of K_s (Karoly and Hoskins 1982), which shows a monotonic increase into the stratosphere over most of the study region (not shown). More detailed analysis of the vertical propagation of the wave activity, using localized Eliassen–Palm flux and WKB diagnostics, will be needed to quan-

tify the effect of the basic-state flow on the evolution of the wave activity isolated in the present study.

Evidence presented here supports the possibility that the upper-level waves may be a source for the generation of equatorially trapped Rossby modes, as has been argued for mixed Rossby–gravity waves (e.g., Magaña and Yanai 1995). This is supported by additional regression analyses using 200-mb vorticity as a predictor (not shown), which indicate that 850-mb cyclonic anomalies preferentially occur to the west of upper-level cyclonic anomalies, as in Figs. 1 and 3. Thus the upper-level waves may help determine the spatial and temporal scale selection of the equatorial Rossby modes, which also have a preferred period in the 12–15-day range.

In addition, the presence of convection at low latitudes might also play a role in the spinup of the equatorial Rossby mode. In any event, the accompanying mass circulation should significantly alter the vertical structure. Yet the perturbations do not project substantially onto the first baroclinic mode, even in the vicinity of the convection. This is in agreement with the observation of Kiladis and Wheeler (1995) that the equatorial Rossby wave perturbations were of the same sign throughout the entire depth of the troposphere. However, in that study it was also found that the OLR signal propagated westward along with the equatorial Rossby wave signal, whereas in Fig. 3 the OLR signal shows eastward propagation. A series of primitive equation model experiments is currently being designed to test the impact of convection on the development of both the upper- and lower-level Rossby waves at low latitudes.

At least some of the interannual variability in the wave activity can be related to changes in the large-scale circulation induced by SST anomalies associated with the Southern Oscillation. Synoptic experience suggests that this modulation occurs at intraseasonal timescales as well. This could be due to low-frequency fluctuations in the jet and storm track source regions of the wave activity, or to slowly evolving large-scale tropical circulations, such as those associated with the MJO. Such temporal-scale interaction within the Tropics is a topic that certainly warrants further investigation.

Acknowledgments. Discussions with Klaus Weickmann, Brian Hoskins, Adrian Matthews, and Matthew Wheeler provided valuable insights into the observational results of this study. Comments by Ken Gage, Haig Iskenderian, and Leslie Hartten, as well as the careful reading by two reviewers of an earlier draft of the paper led to substantial improvements in interpretation and presentation. This research was supported by the Pan-American Climate Studies (PACS) Program under Project GC95-820, sponsored by NOAA's Office of Global Programs.

REFERENCES

Arkin, P. A., 1989: The global climate for December 1988–February 1989: Cold episode in the tropical Pacific continues. *J. Climate*, **2,** 737–757.

——, and P. J. Webster, 1985: Annual and interannual variability of tropical–extratropical interaction. *Mon. Wea. Rev.*, **113,** 1510–1523.

Chang, H.-R., and P. J. Webster, 1990: Energy accumulation and emanation at low latitudes. Part II: Nonlinear response to strong episodic equatorial forcing. *J. Atmos. Sci.*, **47,** 2624–2644.

——, and P. J. Webster, 1995: Energy accumulation and emanation at low latitudes. Part III: Forward and backward accumulation. *J. Atmos. Sci.*, **52,** 2384–2403.

Gage, K. S., J. R. McAfee, D. A. Carter, W. L. Ecklund, A. C. Riddle, G. C. Reid, and B. B. Balsley, 1991: Long-term mean vertical motion over the tropical Pacific: Wind-profiling Doppler radar measurements. *Science*, **254,** 1771–1773.

Gill, A. E., and E. M. Rasmusson, 1983: The 1982–83 climate anomaly in the equatorial Pacific. *Nature*, **306,** 229–234.

Haynes, P. H., and M. E. McIntyre, 1987: On the evolution of isentropic distributions of potential vorticity in the presence of diabatic heating and frictional or other forces. *J. Atmos. Sci.*, **44,** 828–841.

Hoskins, B. J., and T. Ambrizzi, 1993: Rossby wave propagation on a realistic longitudinally varying flow. *J. Atmos. Sci.*, **50,** 1661–1671.

——, I. N. James, and G. H. White, 1983: The shape, propagation and mean-flow interaction of large-scale weather systems. *J. Atmos. Sci.*, **40,** 1595–1612.

——, M. E. McIntyre, and A. W. Robertson, 1985: On the use and significance of isentropic potential vorticity maps. *Quart. J. Roy. Meteor. Soc.*, **111,** 877–946.

Hsu, H.-H., and S.-H. Lin, 1992: Global teleconnections in the 250-mb streamfunction field during the Northern Hemisphere winter. *Mon. Wea. Rev.*, **120,** 1169–1190.

Iskenderian, H., 1995: A 10-year climatology of Northern Hemisphere tropical cloud plumes and their composite flow patterns. *J. Climate*, **8,** 1630–1637.

Janowiak, J. E., P. A. Arkin, P. Xie, M. L. Morrissey, and D. R. Legates, 1995: An examination of the east Pacific ITCZ rainfall distribution. *J. Climate*, **8,** 2810–2823.

Jeffreys, H., 1926: On the dynamics of geostrophic winds. *Quart. J. Roy. Meteor. Soc.*, **52,** 85–104.

Kalnay, E., and Coauthors, 1996: The NCEP/NCAR 40-year reanalysis project. *Bull. Amer. Meteor. Soc.*, **77,** 437–471.

Karoly, D. J., 1983: Rossby wave propagation in a barotropic atmosphere. *Dyn. Atmos. Oceans*, **7,** 111–125.

——, and B. J. Hoskins, 1982: Three dimensional propagation of planetary waves. *J. Meteor. Soc. Japan*, **60,** 109–123.

Kiladis, G. N., and K. M. Weickmann, 1992a: Circulation anomalies associated with tropical convection during northern winter. *Mon. Wea. Rev.*, **120,** 1900–1923.

——, and ——, 1992b: Extratropical forcing of tropical Pacific convection during northern winter. *Mon. Wea. Rev.*, **120,** 1924–1938.

——, and S. B. Feldstein, 1994: Rossby wave propagation into the tropics in two GFDL general circulation models. *Climate Dyn.*, **9,** 245–252.

——, and M. Wheeler, 1995: Horizontal and vertical structure of observed tropospheric equatorial Rossby waves. *J. Geophys. Res.*, **100,** 22 981–22 997.

——, and K. M. Weickmann, 1997: Horizontal structure and seasonality of large-scale circulations associated with tropical convection. *Mon. Wea. Rev.*, **125,** 1997–2013.

——, G. A. Meehl, and K. M. Weickmann, 1994: Large-scale circulation associated with westerly wind bursts and deep convection over the western equatorial Pacific. *J. Geophys. Res.*, **99,** 18 527–18 544.

Liebmann, B., and H. H. Hendon, 1990: Synoptic-scale disturbances near the equator. *J. Atmos. Sci.,* **47,** 1463–1479.
——, and C. A. Smith, 1996: Description of a complete (interpolated) outgoing longwave radiation dataset. *Bull. Amer. Meteor. Soc.,* **77,** 1275–1277.
Madden, R., and P. Julian, 1994: Observations of the 40–50-day tropical oscillation—A review. *Mon. Wea. Rev.,* **122,** 814–837.
Magaña, V., and M. Yanai, 1995: Mixed Rossby–gravity waves triggered by lateral forcing. *J. Atmos. Sci.,* **52,** 1473–1486.
Mak, M. K., 1969: Laterally driven stochastic motions in the tropics. *J. Atmos. Sci.,* **26,** 41–64.
Matsuno, T., 1966: Quasi-geostrophic motions in the equatorial area. *J. Meteor. Soc. Japan,* **44,** 25–43.
McGuirk, J. P., A. H. Thompson, and N. R. Smith, 1987: Moisture bursts over the tropical Pacific Ocean. *Mon. Wea. Rev.,* **115,** 787–798.
——, ——, and J. R. Schaefer, 1988: An eastern Pacific tropical plume. *Mon. Wea. Rev.,* **116,** 2505–2521.
Meehl, G. A., G. N. Kiladis, K. M. Weickmann, M. Wheeler, D. S. Gutzler, and G. P. Compo, 1996: Modulation of equatorial subseasonal convective episodes by tropical–extratropical interaction in the Indian and Pacific Ocean regions. *J. Geophys. Res.,* **101,** 15 033–15 049.
Mo, K., and E. M. Rasmusson, 1993: The 200-mb vorticity budget during 1986–1989 as revealed by NMC analyses. *J. Climate,* **6,** 577–594.
Newell, R. E., J. W. Kidson, D. G. Vincent, and G. J. Boer, 1972: *The General Circulation of the Tropical Atmosphere.* Vol. 1. The MIT Press, 258 pp.
——, ——, ——, and ——, 1974: *The General Circulation of the Tropical Atmosphere.* Vol. 2. MIT Press, 371 pp.
Starr, V. P., 1948: An essay on the general circulation of the earth's atmosphere. *J. Meteor.,* **5,** 39–48.
Takayabu, Y. N., 1994: Large-scale cloud disturbances associated with equatorial waves. Part I: Spectral features of the cloud disturbances. *J. Meteor. Soc. Japan,* **72,** 433–448.
Thorncroft, C. D., B. J. Hoskins, and M. E. McIntyre, 1993: Two paradigms of baroclinic-wave life-cycle behaviour. *Quart. J. Roy. Meteor. Soc.,* **119,** 17–55.
Tomas, R. A., and P. J. Webster, 1994: Horizontal and vertical structure of cross-equatorial wave propagation. *J. Atmos. Sci.,* **51,** 1417–1430.
Wallace, J. M., and N.-C. Lau, 1985: On the role of barotropic energy conversions in the general circulation. *Advances in Geophysics,* Vol. 28, Academic Press, 33–74.
Webster, P. J., and H.-R. Chang, 1988: Equatorial energy accumulation and emanation regions: Impacts of a zonally varying basic state. *J. Atmos. Sci.,* **45,** 803–829.
——, and J. R. Holton, 1982: Cross-equatorial response to middle-latitude forcing in a zonally varying basic state. *J. Atmos. Sci.,* **39,** 722–733.
Weickmann, K. M., G. N. Kiladis, and P. D. Sardeshmukh, 1997: The dynamics of intraseasonal atmospheric angular momentum oscillations. *J. Atmos. Sci.,* **54,** 1445–1461.
Wilson, J. D., and M. K. Mak, 1984: Tropical response to lateral forcing with a latitudinally and zonally nonuniform basic state. *J. Atmos. Sci.,* **41,** 1187–1201.
Yanai, M., and M.-M. Lu, 1983: Equatorially trapped waves at the 200-mb level and their association with meridional convergence of wave energy flux. *J. Atmos. Sci.,* **40,** 2785–2803.
Yang, G.-Y, and B. J. Hoskins, 1996: Propagation of Rossby waves of nonzero frequency. *J. Atmos. Sci.,* **53,** 2365–2378.
Zangvil, A., and M. Yanai, 1980: Upper tropospheric waves in the tropics. Part I: Dynamical analysis in the wavenumber-frequency domain. *J. Atmos. Sci.,* **37,** 283–298.
——, and ——, 1981: Upper tropospheric waves in the tropics. Part II: Association with clouds in the wavenumber-frequency domain. *J. Atmos. Sci.,* **38,** 939–953.
Zhang, C., and P. J. Webster, 1992: Laterally forced equatorial perturbations in a linear model. Part I: Stationary transient forcing. *J. Atmos. Sci.,* **49,** 585–607.